

**Next-To-Leading Order Differential Cross-Sections for J/ψ ,
 $\psi(2S)$ and Υ Production in Proton-Proton Collisions at a
Fixed-Target Experiment using the LHC Beams (AFTER@LHC)**

Yu Feng and Jian-Xiong Wang

*Institute of High Energy Physics, Chinese Academy
of Sciences, P.O.Box 918(4), Beijing 100049, China.*

Abstract

Using nonrelativistic QCD (NRQCD) factorization, we calculate the yields for J/ψ , $\psi(2S)$ and $\Upsilon(1S)$ hadroproduction at $\sqrt{s} = 72$ GeV and 115 GeV including the next-to-leading order QCD corrections. Both these center-of-mass energies correspond to those obtained with 7 TeV and 2.76 TeV nucleon beam impinging a fixed target. We study the cross section integrated in p_t as a function of the rapidity as well as the p_t differential cross section in the central rapidity region. Using different NLO fit results of the NRQCD long-distance matrix elements, we evaluate a theoretical uncertainty which is certainly much larger than the projected experimental uncertainties with the expected 20 fb^{-1} to be collected per year with AFTER@LHC.

PACS numbers: 12.38.Bx, 13.60.Le, 13.88.+e, 14.40.Pq

I. INTRODUCTION

Non-relativistic quantum chromodynamics (NRQCD) [1] is the most systematic factorization scheme to describe the decay and production of heavy quarkonia. It allows one to organize the theoretical calculations as double expansions in both the coupling constant α_s and the heavy-quark relative velocity v . In the past few years, significant progress has been made in next-to-leading order (NLO) QCD calculations based on NRQCD. Calculations and fits of NRQCD long-distance matrix elements (LDMEs) for both the J/ψ yield and polarization in hadroproduction have been carried out [2–6] as well as for Υ hadroproduction [7, 8]. Using these LDMEs, one can in principle predict the transverse momentum p_t differential cross section at any energies. In addition, in a recent study [9], we have discussed the implication of these fits on the energy dependence of the cross sections integrated in p_t .

In this paper, we predict these differential cross sections for the kinematics of a fixed-target experiment using the LHC beams (AFTER@LHC) [10]. In practice, 7 TeV protons on targets yield to a c.m.s energy close to 115 GeV and 72 GeV for 2.76 TeV nucleons (as in the case of a Pb beam). This corresponds to a range very seldom explored so far, significantly higher than that at CERN-SPS and not far from BNL-RHIC. With the typical luminosity of the fixed-target mode, which allows for yearly luminosities as large as 20 fb^{-1} , AFTER@LHC is expected to be a quarkonium and heavy-flavor observatory [10, 11]. In general, the opportunities of a fixed-target experiment using the LHC beam for spin and heavy-ion physics are discussed in [10, 12–14]. In this work, we confirm that charmonium yields can easily reach 10^9 per year and 10^6 for bottomonia.

II. NEXT-TO-LEADING ORDER CALCULATION

Following the NRQCD factorization formalism [1], the cross section for quarkonium hadroproduction H can be expressed as

$$d\sigma[pp \rightarrow H + X] = \sum_{i,j,n} \int dx_1 dx_2 G_p^i G_p^j d\hat{\sigma}[ij \rightarrow (Q\bar{Q})_n X] \langle \mathcal{O}_n^H \rangle \quad (1)$$

where p is either a proton or an antiproton, $G_p^{i(j)}$ is the parton distribution function (PDF) of p , the indices i, j runs over all possible partonic species, and n denotes the color, spin and angular momentum states of the intermediate $Q\bar{Q}$ pair. For ψ and Υ , namely the 3S_1

quarkonium states, their leading CO states of relative order $\mathcal{O}(v^4)$ are $^1S_0^{[8]}$, $^3S_1^{[8]}$, $^3P_J^{[8]}$. Along with the CS transition $^3S_1^{[1]}$, we call the total CS + CO contributions as direct production. The short-distance coefficient (SDC) $d\hat{\sigma}$ will be calculated perturbatively, while the long-distance matrix elements (LDMEs) $\langle \mathcal{O}_n^H \rangle$ are governed by nonperturbative QCD effects.

Now let us take a look at the parton level processes related in this work. As we know that, for hadroproduction, the CO contributions appear at α_s^2 [15], their Born contributions are

$$\begin{aligned} q + \bar{q} &\rightarrow Q\bar{Q}[^3S_1^{[8]}], \\ g + g &\rightarrow Q\bar{Q}[^1S_0^{[8]}, ^3P_{J=0,2}^{[8]}], \end{aligned} \quad (2)$$

where $q(\bar{q})$ denotes the light quarks (antiquarks).

Up to α_s^3 , QCD corrections include real and virtual parts. One inevitably encounters ultra-violet (UV), infra-red(IR) and Coulomb divergences when dealing the virtual corrections. UV divergences from self-energy and triangle diagrams are canceled upon the renormalization procedure. For the real emission corrections, three kinds of processes are contained

$$\begin{aligned} g + g &\rightarrow Q\bar{Q}[^3S_1^{[1]}, ^1S_0^{[8]}, ^3S_1^{[8]}, ^3P_{J=0,2}^{[8]}] + g, \\ g + q(\bar{q}) &\rightarrow Q\bar{Q}[^1S_0^{[8]}, ^3S_1^{[8]}, ^3P_{J=0,2}^{[8]}] + q(\bar{q}), \\ q + \bar{q} &\rightarrow Q\bar{Q}[^1S_0^{[8]}, ^3S_1^{[8]}, ^3P_{J=0,1,2}^{[8]}] + g. \end{aligned} \quad (3)$$

some of which involve IR singularities in phase-space integration and we adopt the two-cutoff phase space slicing method [16] to isolate these singularities by introducing two small cutoffs, δ_s and δ_c . For technique details, we refer readers to Ref. [17, 18].

One has to note that in Eq.(3), the $^3S_1^{[1]}$ production in gg fusion is not really correction, strictly speaking, it is only the Born order contribution for hadroproduction with a jet. In fact, all the real emission processes in Eq.(3) will be taken as Born-order contributions of quarkonium - jet production. Then one can discuss the p_t dependent differential cross section and, the QCD NLO corrections in this case are up to α_s^4 , which involves real emission

processes

$$\begin{aligned}
g + g &\rightarrow (Q\bar{Q})_n + g + g, & g + g &\rightarrow (Q\bar{Q})_n + q + \bar{q}, \\
g + q(\bar{q}) &\rightarrow (Q\bar{Q})_n + g + q(\bar{q}), & q + \bar{q} &\rightarrow (Q\bar{Q})_n + g + g, \\
q + \bar{q} &\rightarrow (Q\bar{Q})_n + q + \bar{q}, & q + \bar{q} &\rightarrow (Q\bar{Q})_n + q' + \bar{q}', \\
q + q &\rightarrow (Q\bar{Q})_n + q + q, & q + q' &\rightarrow (Q\bar{Q})_n + q + q'.
\end{aligned} \tag{4}$$

where q, q' denote light quarks with different flavors and $(Q\bar{Q})_n$ can be either $^3S_1^{[1]}$, $^1S_0^{[8]}$, $^3S_1^{[8]}$, or $^3P_J^{[8]}$. One can find the detailed descriptions at this order in Ref. [18, 19] and some examples [2, 3, 6–8].

All of these calculations are made with the newly-updated Feynman Diagram Calculation package [20].

III. CONSTRAINS ON THE LDMEs

The color-singlet (CS) LDMEs are estimated from wave functions at the origin by $\langle \mathcal{O}^H(^3S_1^{[1]}) \rangle = \frac{3N_c}{2\pi} |R_H(0)|^2$, where the wave functions are obtained via potential model calculation [21], which gives $|R_{J/\psi}(0)|^2 = 0.81 \text{ GeV}^3$, $|R_{\psi(2S)}(0)|^2 = 0.53 \text{ GeV}^3$, $|R_{\Upsilon(1S)}(0)|^2 = 6.5 \text{ GeV}^3$. We note this part as CSM results when performed separately in the following context.

For the color-octet (CO) LDMEs, they can only be extracted from data. Due to the improvements of NLO calculation, groups of LDMEs based on NLO corrections are obtained by different fitting schemes. Some of them are used in this work as the theoretical uncertainty and we will give a brief discussion on these CO LDMEs below.

In the J/ψ case, seven groups of LDMEs [2, 5, 6, 22–25] are collected in Table. I. They are extracted by fitting the data of hadroproduction yield [2], or combined with polarization [5, 6] on pp collisions. The first one [22] was based on a wider set of data including ep and $\gamma\gamma$ system with $p_t > 1 \text{ GeV}$. In Ref. [5, 6], the data with $p_t < 7 \text{ GeV}$ are excluded in their fit. The fit in Ref. [23, 24] took the η_c measurement ($p_t \geq 6 \text{ GeV}$) into consideration. Only one of them is used [24] since their results are almost the same. The last one incorporates the leading-power fragmentation corrections together with the QCD NLO corrections, which results in a different SDC and may bring different LDMEs. In Ref. [2], Ma *et al.* fit the data

with $p_t > 7$ GeV by two linear combinations of LDMEs:

$$\begin{aligned} M_{0,r_0}^{J/\psi} &= \langle \mathcal{O}^{J/\psi}(^1S_0^{[8]}) \rangle + \frac{r_0}{m_c^2} \langle \mathcal{O}^{J/\psi}(^3P_0^{[8]}) \rangle \\ M_{1,r_1}^{J/\psi} &= \langle \mathcal{O}^{J/\psi}(^3S_1^{[8]}) \rangle + \frac{r_1}{m_c^2} \langle \mathcal{O}^{J/\psi}(^3P_0^{[8]}) \rangle \end{aligned} \quad (5)$$

where we extract the value of LDMEs by limiting $\langle \mathcal{O}^{J/\psi}(^1S_0^{[8]}) \rangle$ and $\langle \mathcal{O}^{J/\psi}(^3S_1^{[8]}) \rangle$ to be positive to get a loose constraint on the $\langle \mathcal{O}^{J/\psi}(^3P_0^{[8]}) \rangle$ range, from which we choose the middle value to obtain the three LDMEs ($Ma(2011)$ in Table. I).

TABLE I: The values of LDMEs for J/ψ hadroproduction (in units of GeV^3).

Ref.	$\langle \mathcal{O}^{J/\psi}(^3S_1^{[1]}) \rangle$	$\langle \mathcal{O}^{J/\psi}(^1S_0^{[8]}) \rangle$	$\langle \mathcal{O}^{J/\psi}(^3S_1^{[8]}) \rangle$	$\langle \mathcal{O}^{J/\psi}(^3P_0^{[8]}) \rangle / m_Q^2$
Butenschoen(2011) [22]	1.32	3.0×10^{-2}	1.7×10^{-3}	-4.0×10^{-3}
Chao(2012) [5]	1.16	8.9×10^{-2}	3.0×10^{-3}	5.6×10^{-3}
Ma(2011) [2]	1.16	3.9×10^{-2}	5.6×10^{-3}	8.9×10^{-3}
Gong(2013) [6]	1.16	9.7×10^{-2}	-4.6×10^{-3}	-9.5×10^{-3}
Zhang(2015) [23]	$0.24 \sim 0.90$	$(0.4 \sim 1.1) \times 10^{-2}$	1.0×10^{-2}	1.7×10^{-2}
Han(2015) [24]	1.16	0.7×10^{-2}	1.0×10^{-2}	1.7×10^{-2}
Bodwin(2014) [25]	0	9.9×10^{-2}	1.1×10^{-2}	4.9×10^{-3}

As regards the $\psi(2S)$, only two NLO analyses results in Ref. [2, 6] are used, both of which excluded the data with $p_t < 7$ GeV in their fit. To extract the LDMEs value from the fitting results of Ma *et al.*, the same method is used as for the J/ψ . For $\Upsilon(1S)$, we use three groups of LDMEs [8, 26, 27]. Both of them have separated the direct production and

TABLE II: The values of LDMEs for $\psi(2S)$ and $\Upsilon(1S)$ hadroproduction (in units of GeV^3).

H	Ref.	$\langle \mathcal{O}^H(^3S_1^{[1]}) \rangle$	$\langle \mathcal{O}^H(^1S_0^{[8]}) \rangle$	$\langle \mathcal{O}^H(^3S_1^{[8]}) \rangle$	$\langle \mathcal{O}^H(^3P_0^{[8]}) \rangle / m_Q^2$
$\psi(2S)$	Gong(2013) [6]	0.76	-1.2×10^{-4}	3.4×10^{-3}	4.2×10^{-3}
	Ma(2011) [2]	0.76	1.4×10^{-2}	2.0×10^{-3}	1.6×10^{-3}
$\Upsilon(1S)$	Gong(2014) [8]	9.28	11.2×10^{-2}	-4.1×10^{-3}	-6.7×10^{-3}
	Han(2014) [26]	9.28	3.5×10^{-3}	5.8×10^{-2}	3.6×10^{-2}
	Feng(2015) [27]	9.28	13.6×10^{-2}	6.1×10^{-3}	-9.3×10^{-3}

the feed-down contributions exactly. In the fit of Ref. [26], only the data in $p_t > 15$ GeV region are used, while in Ref. [8, 27] the region is $p_t > 8$ GeV. They all describe the high p_t yield data at Tevatron and LHC very well. We gather the LDMEs of $\psi(2S)$ and $\Upsilon(1S)$ in Table. II.

IV. NUMERICAL RESULTS

The differential cross sections with rapidity distribution and transverse momentum distribution are considered in the calculation. In both cases, the CTEQ6M parton distribution functions [28] and corresponding two-loop QCD coupling constants α_s are used. The charm quark mass is set to be $m_c = 1.5$ GeV, while for bottom quark it is $m_b = 4.75$ GeV. The renormalization and factorization scales are chosen as $\mu_r = \mu_f = 2m_Q$ for rapidity distribution plots, while for the plots of transverse momentum distribution they are $\mu_r = \mu_f = \mu_T$, with $\mu_T = \sqrt{(2m_Q)^2 + p_t^2}$. NRQCD scale is chosen as $\mu_\Lambda = m_Q$. It is important to note that different choices of these scales may be adopted for the CO LDMEs we used from different groups, which can bring some uncertainties in our prediction. The uncertainties from scales and quark masses are also considered for cross sections with rapidity distribution, where scale dependence is estimated by varying μ_r, μ_f , by a factor of 1/2 and 2 with respect to their central values and quark masses varying 0.1 GeV up and down for J/ψ , as well as 0.25 GeV for Υ . Branching ratios are taken from PDG [29], which give $\mathcal{B}[J/\psi \rightarrow \mu\mu] = 0.0596$, $\mathcal{B}[\psi(2S) \rightarrow \mu\mu] = 0.0079$ and $\mathcal{B}[\Upsilon(1S) \rightarrow \mu\mu] = 0.0248$, respectively. The two phase space cutoffs $\delta_s = 10^3$ and $\delta_c = \delta_s/50$ are chosen and the insensitivity of the results on different choices for these cutoffs has been checked.

A. $d\sigma/dy$ up to α_s^3

We study the p_t integrated cross section (where the whole p_t region are integrated) as a function of rapidity in this subsection. The QCD NLO corrections are up to α_s^3 here. In Fig. 1 and Fig. 2, we perform the rapidity distribution of direct J/ψ , $\psi(2S)$ and $\Upsilon(1S)$ production cross section at center of mass energy $\sqrt{s} = 72$ GeV and 115 GeV, respectively. We first discuss the branching contributions shown in Fig. 1, where the CO LDMEs are set to unity for all three production channels. For $\psi(2S)$, the CSM is different from J/ψ only

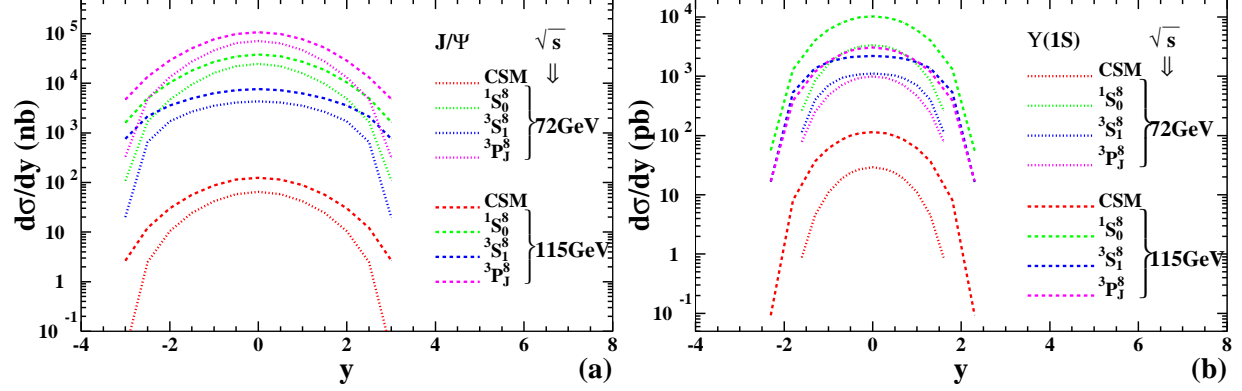


FIG. 1: Branching contributions of the cross section for direct J/ψ (left) and $\Upsilon(1S)$ (right) hadroproduction at the c.m.s energy 72 GeV (dot lines) and 115 GeV (dashed lines), respectively. The CO LDMEs for all the channels are set to unity.

by a factor, we therefore do not perform it separately. Obviously, the CSM results (red lines) for both J/ψ and $\Upsilon(1S)$ is small compared with the CO channels. The dominant CO channel for J/ψ is $^3P_J^{[8]}$ transition, while for $\Upsilon(1S)$ it is $^1S_0^{[8]}$. Besides, the branching contributions for J/ψ have visible hierarchy, but for $\Upsilon(1S)$, little difference between $^3S_1^{[8]}$ and $^3P_J^{[8]}$ contributions.

Adopting the LDMEs in Table. I and II, we present the rapidity distribution of cross section for various cases in Fig. 2. The lines are the central values with different groups of LDMEs, while the colored areas are the uncertainties from scales and quark masses. Only the boundary lines are shown with scales and mass uncertainties. For the J/ψ , six groups of NRQCD results are shown as a band, the boundaries of which has a distance within factor 10. The values of the cross sections are roughly in the region of $10^4 \sim 10^5$ pb. The CSM results lower than the band, again by a factor 10. Without a surprise, the CSM seems to be negligible for total NRQCD results. However, it may not be the case. In fact, as we have discussed in Ref. [9], the LO CSM contribution explains the data very well from the RHIC to LHC energies, while the CO LDMEs extracted from p_t -differential NLO correction would lead to the p_t -integrated cross section overshooting the data. Only the fits from Butenschoen *et al.* [22] that including rather low p_t data provides an acceptable description of the p_t -integrated cross section. Based on these discussion, most of the predictions in Fig. 2 might overshoot the data and CSM may underestimate the measurements below RHIC energy. For various groups of the LDMEs, they are fitted with large p_t data, while in our calculation the

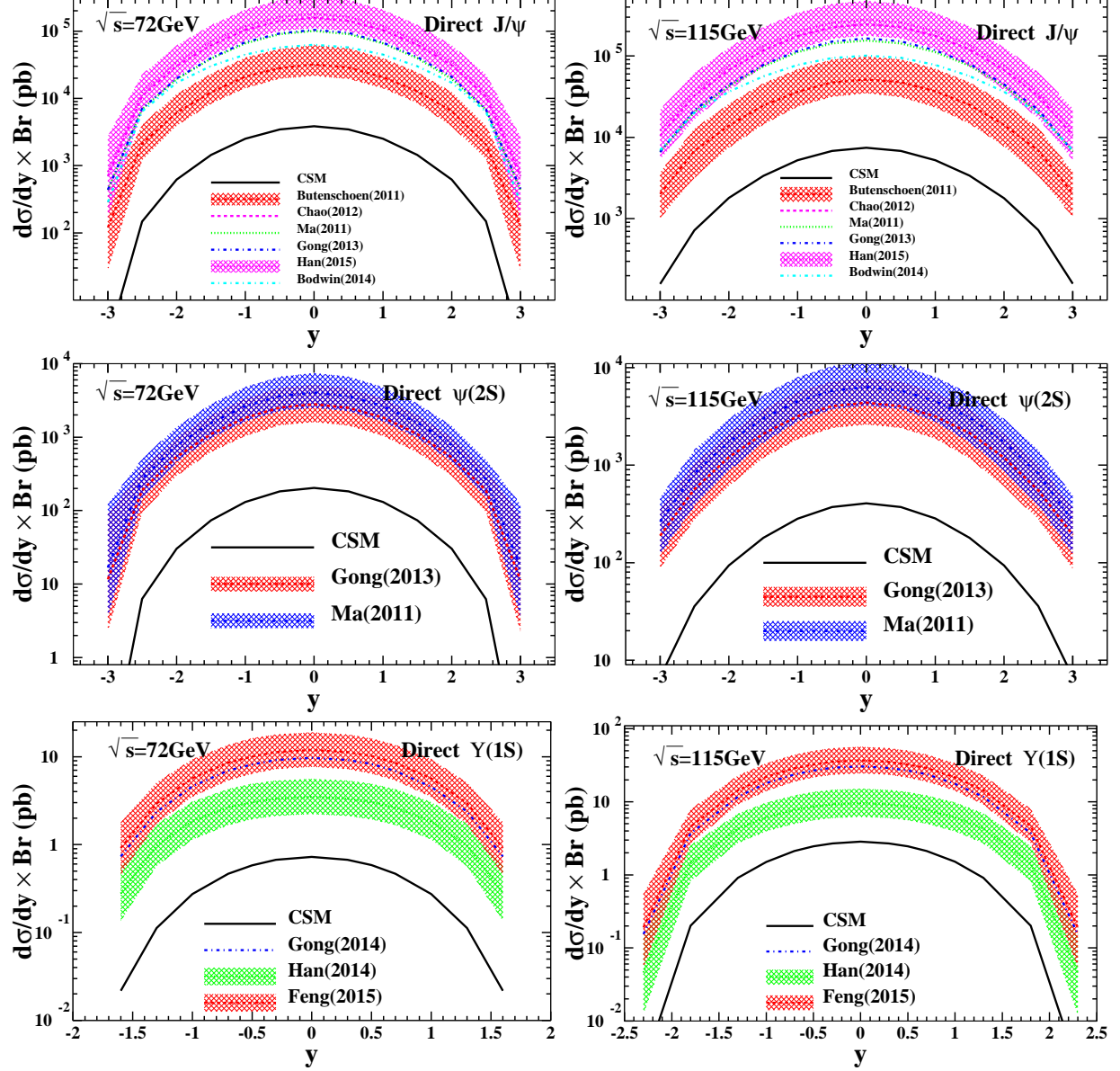


FIG. 2: Rapidity distribution of differential cross section for direct J/ψ (top), $\psi(2S)$ (middle) and $\Upsilon(1S)$ (bottom) hadroproduction at the center of mass energy $\sqrt{s} = 72$ GeV and $\sqrt{s} = 115$ GeV, respectively. The lines are the uncertainty from LDMEs values while the color areas are scales and masses uncertainties.

whole p_t region are integrated. We suppose the one of Butenschoen *et al.* [22], namely the lower boundary of the band (red dashed line) would give a best prediction for J/ψ , though their LDMEs will meet difficulty when describing the polarization data.

As regards the $\psi(2S)$, two groups of LDMEs lead to a consistent predictions which give the cross section around 10^3 pb at both $\sqrt{s} = 72$ GeV and 115 GeV. With the uncertainties

of scales and quark masses, the cross sections reach 10^4 pb in the central rapidity region. Nevertheless, these results overestimated the data as discussed in Ref. [9].

In the $\Upsilon(1S)$ case, two curves are close and the left one is slightly departure. Yet, their difference is only in pb units. We ever performed a quite good prediction for $\Upsilon(1S)$ at RHIC energies and below [9], which includes the energies we considered here.

B. $d\sigma/dp_t$ up to α_s^4

Now let us discuss the cross sections depend on transverse momentum p_t . In Fig. 3, the p_t distribution of direct J/ψ , $\psi(2S)$ and $\Upsilon(1S)$ hadroproduction are presented. For J/ψ and $\psi(2S)$, the productions are dominated by the CO contributions, which is larger than CSM at least one order of magnitudes that the latter one would be negligible. The various groups of LDMEs predict J/ψ and $\psi(2S)$ hadroproduction in a consistent way that the uncertainty band among them is very narrow. Only the one from Ref. [25] (the light blue dot-dashed line) seems to have deviated from the uncertainty band with a larger factor 2 to 10 in J/ψ case. This may be understood by the fact that the fits in Ref. [25] has a different SDC compared with others, which would be the source of large uncertainty.

For $\Upsilon(1S)$, the red dashed and blue dot-dashed lines are almost parallel with little distance, while the green dot line is obviously lower at low p_t region and crosses the other ones as p_t increasing. This may explains the behavior of $d\sigma/dy$ in Fig. 2, that the low p_t difference between the green curve and the other two leads the visible distance after p_t integrating.

V. SUMMARY

We calculated the NLO QCD correction for direct J/ψ , $\psi(2S)$ and $\Upsilon(1S)$ production at fixed-target energies. By using the LHC beams (AFTER@LHC), we can predict the differential cross sections for the kinematics of a fix-target experiment. We studied the cross section integrated in p_t as a function of the rapidity as well as the p_t differential cross section in the central rapidity region, which are up to QCD α_s^3 and α_s^4 corrections, respectively. To perform a reliable prediction, various groups of NRQCD long distance matrix elements by different fitting methods are considered as well as the uncertainties from scales and quark masses. The results are in a consistent that the uncertainties among them is narrow. With

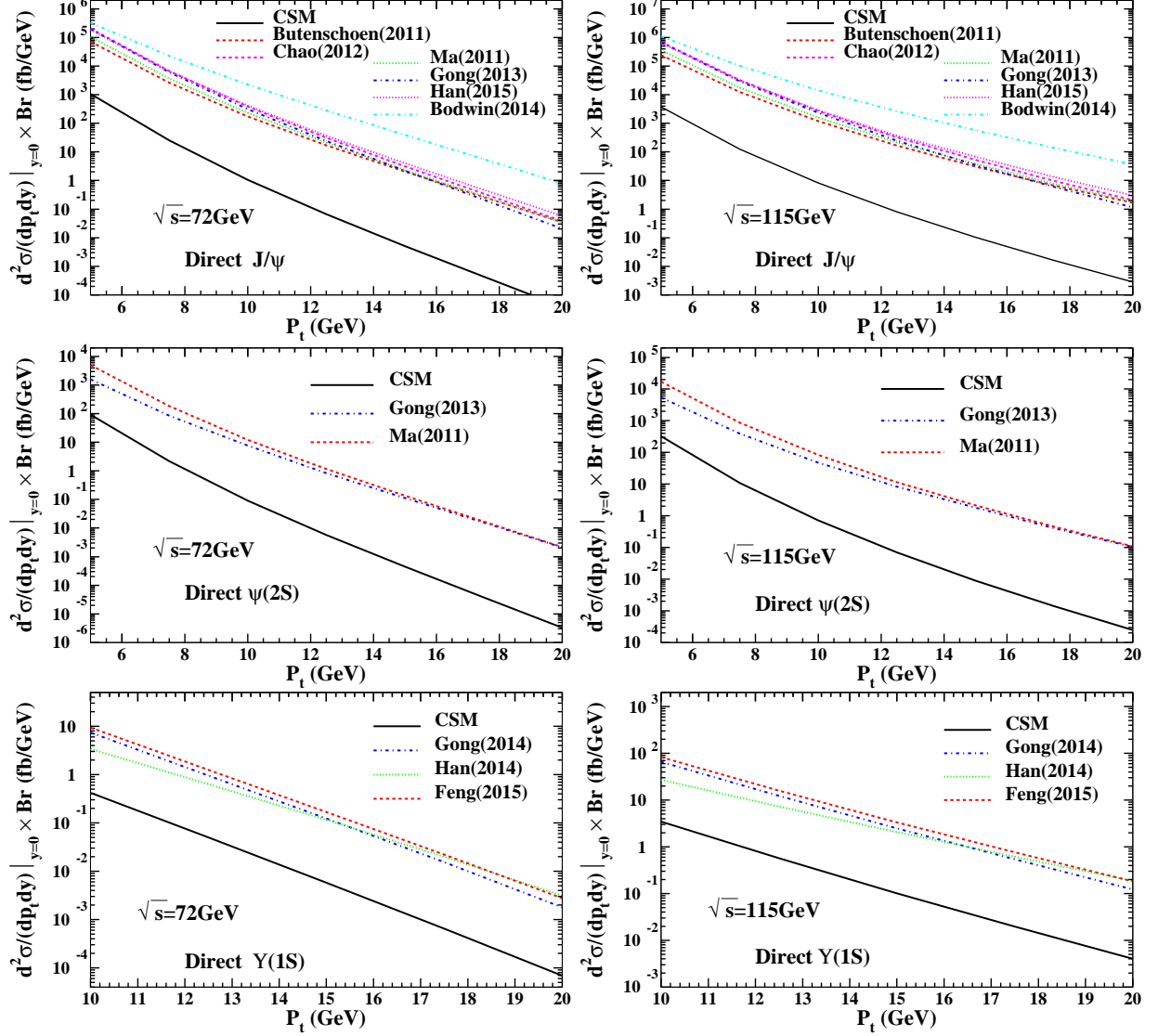


FIG. 3: Transverse momentum distribution of differential cross section with the rapidity $y = 0$ for direct J/ψ , $\psi(2S)$ and $\Upsilon(1S)$ hadroproduction from top to bottom, respectively.

the typical luminosity of the fixed-target mode, which allows for yearly luminosities as large as 20 fb^{-1} for both energy, our predictions confirm that charmonium yields can easily reach 10^9 per year and 10^6 for bottomonia.

Acknowledgments

We are grateful to Jean-Philippe Lansberg for his generous help in this work.

-
- [1] G. T. Bodwin, E. Braaten, and G. P. Lepage, Phys.Rev. **D51**, 1125 (1995), hep-ph/9407339.
 - [2] Y.-Q. Ma, K. Wang, and K.-T. Chao, Phys.Rev.Lett. **106**, 042002 (2011), 1009.3655.
 - [3] M. Butenschoen and B. A. Kniehl, Phys.Rev.Lett. **106**, 022003 (2011), 1009.5662.
 - [4] M. Butenschoen and B. A. Kniehl, Phys.Rev.Lett. **108**, 172002 (2012), 1201.1872.
 - [5] K.-T. Chao, Y.-Q. Ma, H.-S. Shao, K. Wang, and Y.-J. Zhang, Phys.Rev.Lett. **108**, 242004 (2012), 1201.2675.
 - [6] B. Gong, L.-P. Wan, J.-X. Wang, and H.-F. Zhang, Phys.Rev.Lett. **110**, 042002 (2013), 1205.6682.
 - [7] K. Wang, Y.-Q. Ma, and K.-T. Chao, Phys.Rev. **D85**, 114003 (2012), 1202.6012.
 - [8] B. Gong, L.-P. Wan, J.-X. Wang, and H.-F. Zhang, Phys.Rev.Lett. **112**, 032001 (2014), 1305.0748.
 - [9] Y. Feng, J.-P. Lansberg, and J.-X. Wang (2015), 1504.00317.
 - [10] S. Brodsky, F. Fleuret, C. Hadjidakis, and J. Lansberg, Phys.Rept. **522**, 239 (2013), 1202.6585.
 - [11] J. Lansberg, S. Brodsky, F. Fleuret, and C. Hadjidakis, Few Body Syst. **53**, 11 (2012), 1204.5793.
 - [12] L. Massacrier, M. Anselmino, R. Arnaldi, S. Brodsky, V. Chambert, et al. (2015), 1502.00984.
 - [13] J. Lansberg, M. Anselmino, R. Arnaldi, S. Brodsky, V. Chambert, et al., EPJ Web Conf. **85**, 02038 (2015), 1410.1962.
 - [14] A. Rakotozafindrabe, R. Arnaldi, S. Brodsky, V. Chambert, J. Didelez, et al., Nucl.Phys. **A904-905**, 957c (2013), 1211.1294.
 - [15] P. L. Cho and A. K. Leibovich, Phys.Rev. **D53**, 6203 (1996), hep-ph/9511315.
 - [16] B. Harris and J. Owens, Phys.Rev. **D65**, 094032 (2002), hep-ph/0102128.
 - [17] B. Gong and J.-X. Wang, Phys.Rev. **D78**, 074011 (2008), 0805.2469.
 - [18] B. Gong, X. Q. Li, and J.-X. Wang, Phys.Lett. **B673**, 197 (2009), 0805.4751.
 - [19] B. Gong, J.-X. Wang, and H.-F. Zhang, Phys.Rev. **D83**, 114021 (2011), 1009.3839.
 - [20] J.-X. Wang, Nucl.Instrum.Meth. **A534**, 241 (2004), hep-ph/0407058.

- [21] E. J. Eichten and C. Quigg, Phys.Rev. **D52**, 1726 (1995), hep-ph/9503356.
- [22] M. Butenschoen and B. A. Kniehl, Phys.Rev. **D84**, 051501 (2011), 1105.0820.
- [23] H.-F. Zhang, Z. Sun, W.-L. Sang, and R. Li, Phys.Rev.Lett. **114**, 092006 (2014), 1412.0508.
- [24] H. Han, Y.-Q. Ma, C. Meng, H.-S. Shao, and K.-T. Chao, Phys.Rev.Lett. **114**, 092005 (2015), 1411.7350.
- [25] G. T. Bodwin, H. S. Chung, U.-R. Kim, and J. Lee, Phys.Rev.Lett. **113**, 022001 (2014), 1403.3612.
- [26] H. Han, Y.-Q. Ma, C. Meng, H.-S. Shao, Y.-J. Zhang, et al. (2014), 1410.8537.
- [27] Y. Feng, B. Gong, L.-P. Wan, and J.-X. Wang (2015), 1503.08439.
- [28] J. Pumplin, D. Stump, J. Huston, H. Lai, P. M. Nadolsky, et al., JHEP **0207**, 012 (2002), hep-ph/0201195.
- [29] K. Olive et al. (Particle Data Group), Chin.Phys. **C38**, 090001 (2014).